Pak. J. Bot., 58(1) January 2026.

ARTICLE | DOI: http://dx.doi.org/10.30848/PJB2026-1(13)

ISOLATION, STRUCTURAL CHARACTERIZATION AND BIOACTIVE POTENTIAL OF A NOVEL PECTIC POLYSACCHARIDE DERIVED FROM TOBACCO WASTE

YAN ZHAO[1,2], YANJUN HUANG[1], HONGQIAO LAN[1], QINGHUI WU[1], XIUCAI LIU[1], QIAOLING LI[1], QUANXING ZHENG[1], ZECHUN LIU[1*] AND WEI XIE[1*]

[1]Technology Center, China Tobacco Fujian Industrial Co., Ltd, Xiamen 361021, PR China
[2]College of Chemistry and Chemical Engineering, Xiamen University, Xiamen 361005, PR China
WEI XIE and ZECHUN LIU contribute the same to the article and are the corresponding authors

*Corresponding author's email: lzc10497@fjtic.cn; xw10481@fjtic.cn

Abstract

Across the globe, approximately 200 million tons of tobacco waste are generated annually. Traditional treatment methods generally cause resource waste and environmental pollution. It is worth noting that discarded tobacco leaves are abundant in pectic polysaccharides that comprise 5-12% of their dry weight. In this study, a novel pectic polysaccharide, CSTP5b, was isolated from tobacco waste for the first time. This was achieved via sequential extraction with ammonium oxalate, followed by column chromatography. CSTP5b is composed of 55.23% rhamnogalacturonan-I (RG-I) and 44.77% homogalacturonan (HG) domains. The HG domain exhibits methyl esterification, while the RG-I main chain has branches where galactan and arabinan are linked. Characterized by a sheet-like morphology, CSTP5b exhibits weak crystalline properties and notable thermal stability. Additionally, it demonstrates significant free radical scavenging and hypoglycemic activities. This study elucidates the fine structural characteristics of tobacco pectic polysaccharides. This indicates that tobacco waste may serve as a viable source of low methyl-esterified RG-I-HG type pectin and potential natural antioxidants and hypoglycemic products. These findings offer a novel avenue for the targeted exploration of bioactive components in tobacco by-products.

Key words: Tobacco waste; Pectic polysaccharide; RG-I; HG; Structure; Bioactivity

Introduction

The resource utilization of tobacco waste is a key challenge for sustainable agricultural development. With a global annual production of 200 million tons, tobacco waste is often disposed of through landfill or incineration (Tian *et al.*, 2023). This not only leads to resource waste, but also potentially threatens the ecological environment due to the release of nicotine, tar and other harmful components. Tobacco contains abundant active ingredients, including alkaloids (Wang *et al.*, 2022), sterols (Liu *et al.*, 2020), flavonoids (Docheva *et al.*, 2014), phenols (Wang *et al.*, 2008), solanesol (Wang & Gu, 2018), polysaccharides (Chang *et al.*, 2024), etc. Research indicates that plant pectic polysaccharides display biological activities such as immune regulation (Ho *et al.*, 2016), anti-inflammatory effects (Huang *et al.*, 2024) and intestinal health protection (Kang & Chang, 2024). Tobacco cell walls contain a remarkably higher content of pectic polysaccharides amounting to 15% of dry weight compared with conventional crops (Yang *et al.*, 2022). The unique secondary metabolic environment in tobacco may result in structural differences in its pectin relative to conventional plant sources (Hao *et al.*, 2024). The structure analysis of tobacco polysaccharides is an important prerequisite for illuminating structure-activity relationships. Extensive research has focused on the structures and bioactivities of tobacco polysaccharides (Jing *et al.*, 2016; Ma *et al.*, 2024). However, detailed investigations into the structure of tobacco polysaccharides, especially pectic polysaccharides, and their structure-activity relations remain scarce.

Low methylation HG type pectin can interact with calcium ions (Ca^{2+}) in the cell wall, which creates “egg-box” structures (Braccini & Pérez, 2001; Cardoso *et al.*, 2003). It is difficult to extract these tightly bound pectic polysaccharides with water alone, which thereby leads to a reduced yield. Previous studies have revealed that the yield of pectic polysaccharides can be improved by acid (Kang & Chang, 2024), alkali (Teng *et al.*, 2021) or chelators (Jamsazzadeh Kermani *et al.*, 2014) to a large extent. Compared with the traditional alkaline extraction method, ammonium oxalate as a weak acidic chelating agent could disrupt the calcium bridge connection between pectin and the cell wall without triggering β-elimination reactions (Cui *et al.*, 2020). This facilitates the release of pectic polysaccharides. To date, no relevant report has been made on the extraction of pectic polysaccharides from tobacco leaves using ammonium oxalate.

In this work, CSTP5b, which is a chelator-soluble pectic polysaccharide, was purified from tobacco waste. Its physicochemical properties, structure and morphology were analyzed in detail through multiple analytical instruments. In addition, the antioxidant and hypoglycemic activities of CSTP5b were further investigated. This research provides fresh perspectives on structure-activity relationships, which promotes the development of their use in functional pharmaceuticals.

Received: 23-04-2025 | Revised: 02-08-2025 | Accepted: 08-08-2025 | Online: 02-09-2025

Materials and Methods

Tobacco waste was collected from Fujian Province of China in 2023. DEAE-Fast Flow and Sepharose CL-6B were provided by Aladdin Biotechnology (Aladdin Industrial Corporation, Shanghai, China). All other reagents and chemicals were supplied by Sinopharm Chemical Reagent Co., Ltd. (Beijing, China).

Extraction and purification of tobacco pectic polysaccharides: In this step, 1 kg of dried tobacco waste powder was treated with 95% ethanol at a mass-to-volume ratio of 1:10 at room temperature for 48 hours. A water-soluble polysaccharide fraction termed WSTP was obtained by extracting the retained tobacco powder with distilled water at a 1:16 mass-to-volume ratio at 100°C for 3 hours. Then, 0.5% ammonium oxalate was used at a 1:16 solid/liquid ratio to extract pectic chelator-soluble polysaccharide from the solid residues of the hot water fraction of tobacco leaves, with 4-hour mechanical stirring at 25°C. The extract was concentrated to about 2 L under reduced pressure and centrifuged. The supernatants were precipitated through the addition of a fourfold volume of 95% ethanol and 12-hour incubation at 4℃. After 10-minute centrifugation at 4,000 rpm, the precipitates were dried with 95% and absolute ethanol. The precipitate was gathered and deproteinized by use of Sevag reagent, which yielded around 34 g of crude polysaccharide designated as chelator-soluble pectic polysaccharides (CSTPs).

A DEAE Fast Flow ion exchange column (Ø2.6 × 40 cm) was utilized to separate CSTPs, which produced CSTPN and CSTP5 in sequence. CSTP5 was isolated by Sepharose CL-6B column with 0.1 M sodium chloride (NaCl) as the eluent, which yielded the primary pectin fraction CSTP5b. A record was kept of the elution profiles by measuring uronic acid content using the m-hydroxydiphenyl method.

Monosaccharide composition: The monosaccharide composition of CSTP5b was determined according to the previous report (Peng *et al.*, 2023).

Molecular weight: The molecular weight (Mw) of the purified components was determined via high-performance gel permeation hromatography (HPGPC) using a Shimadzu LC-10A with a differential refractometry detector and a BRT-105-103-101 (8 × 300 mm) column. The experimental parameters were set as follows: an injection volume of 20 µL, a column temperature of 40°C, a flow rate of 0.7 mL/min, 0.05 M NaCl solution as the mobile phase and a CSTP5b concentration of 5 mg/mL. The calibration curve was drawn using dextran standards (2 mg/mL) with multiple molecular weights: 7,380, 10,510, 21,950, 44,520, 109,900, 217,800, 410,200 and 755,900 Da.

Fourier transform infrared and ultraviolet spectroscopy: The experimental procedures were based on previously published reports (Ma *et al.*, 2023).

Morphology analysis: The dried sample was affixed to a conductive carbon film and subjected to about 40-second gold-coating in the chamber of an ion sputterer. The sample was examined in a scanning electron microscope chamber with a 2 kV acceleration voltage.

The crystal structure of CSTP5b was determined using the X-ray diffraction (XRD) pattern. The diffractometer functioned across an angular range of 5-90°. For atomic force microscope (AFM) analysis, the samples were deposited on mica sheets, dried and examined in tapping mode at 25℃.

Analysis of CSTP5b methylation: The methylation of CSTP5b was referenced to literature (Huang *et al.*, 2021).

Nuclear magnetic resonance analysis of CSTP5b: CSTP5b was precisely weighed (20 mg) and dissolved in deuterium oxide (D_2O) (99.8%) with acetone as the internal standard. ^{1}H, ^{13}C, heteronuclear singular quantum correlation (HSQC), correlation spectroscopy (COSY) and nuclear Overhauser effect spectroscopy (NOESY) nuclear magnetic resonance (NMR) spectra were measured on a Bruker Avance 600 MHz NMR spectrometer containing a cryo probe (Bruker Inc., Rheinstetten, Germany).

Thermal stability: A thermogravimetric (TG) analyzer (STA 449C, Netzsch, Germany) was applied to perform TG and differential scanning calorimetry (DSC) analyses.

Antioxidant activity: The antioxidant activity of CSTP5b against 1,1-Diphenyl-2-picrylhydrazyl (DPPH), hydroxyl and 2, 2'-azino-bis(3-ethylbenzothiazoline-6-sulfonic acid) (ABTS) was then assessed in vitro using previously reported methods (Ning *et al.*, 2021).

Hypoglycemic effects: The hypoglycemic effect of CSTP5b was assessed by inhibiting α-glucosidase and α-amylase, and using acarbose as a positive control in accordance with established methods (Sun *et al.*, 2024). CSTP5b (0.5, 1.0, 2.0, 4.0, 6.0 and 8.0 mg/mL) was evaluated in both experiments.

Results and Discussion

Extraction, isolation and purification of CSTPs: CSTPs from tobacco leaves were extracted using ammonium oxalate and subsequently deproteinated via the Sevag method, which achieved a yield of 4.25%. Additionally, CSTPs were purified using DEAE Fast Flow column to separate neutral and acidic polysaccharides. Distilled water and 0.5 M NaCl were used successively for elution to obtain two fractions (CSTPN and CSTP5) (Fig. S1a). CSTP5 was a predominant high-purity constituent in polysaccharide fractions. Therefore, CSTP5 was chosen for further purification with Sepharose CL-6B column chromatography (Fig. S1b). After fractionation, the primary independent fraction CSTP5b was isolated for further analysis.

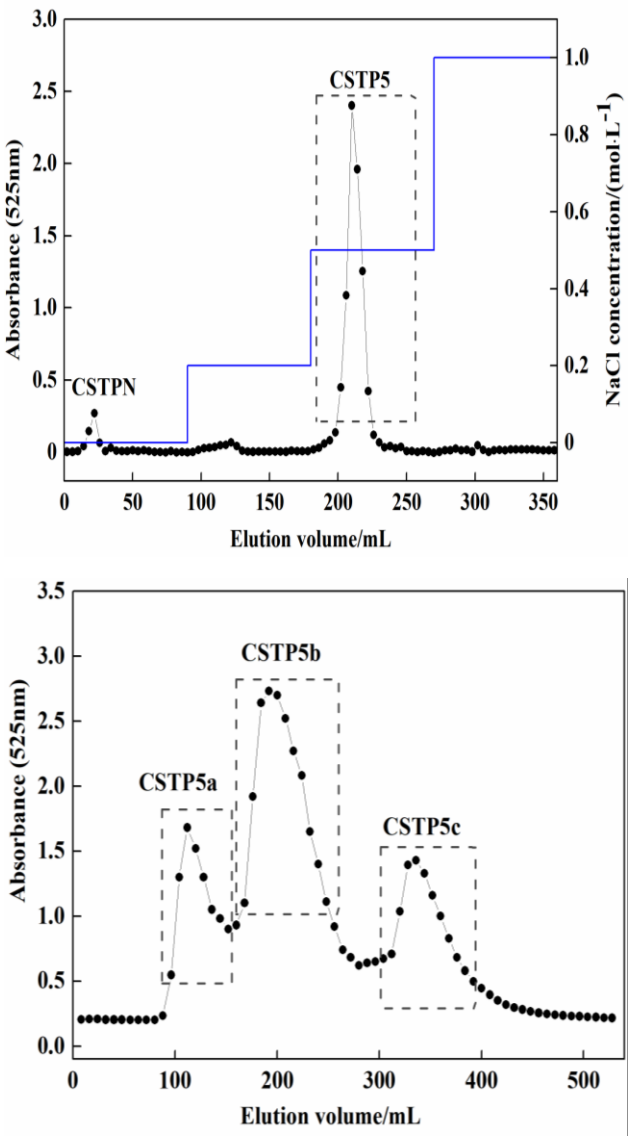

Fig. S1. Column chromatography results of tobacco chelator-soluble polysaccharide. (a) DEAE-Fast Flow column chromatography of CSTP. (b) Sepharose CL-6B column chromatography of CSTP5b.

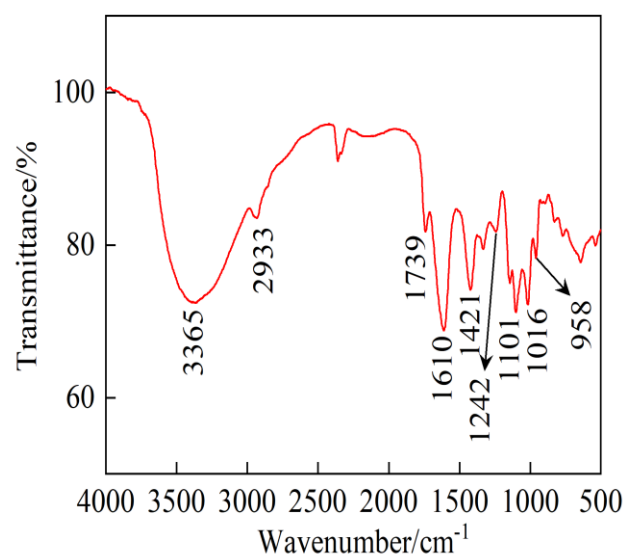

Fig. S2. FT-IR spectrum of CSTP5b.

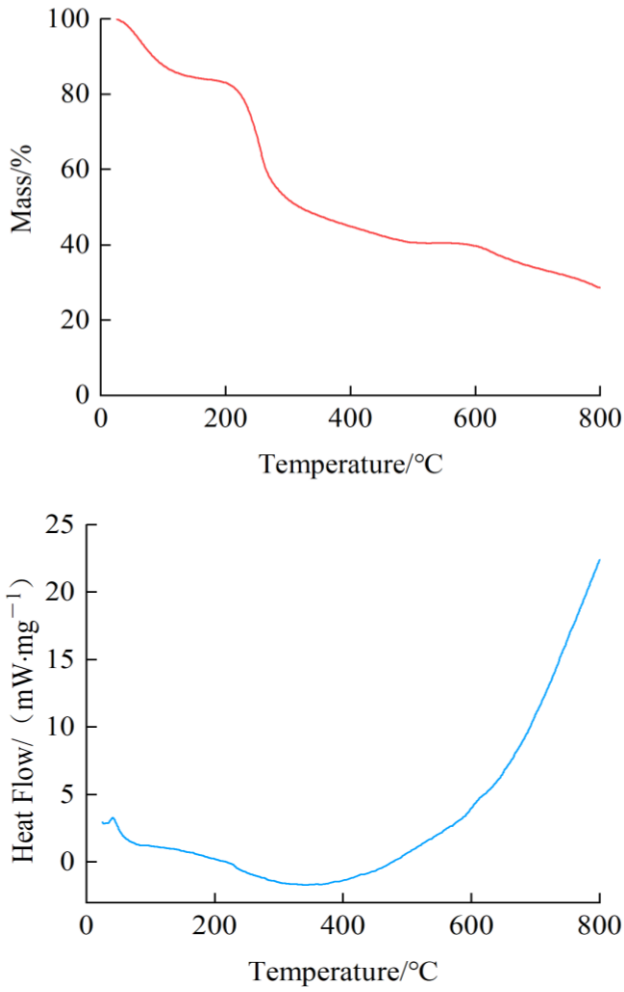

Fig. S3. TG curve (a) and DSC curve (b) of CSTP5b.

Physicochemical characteristics and monosaccharide compositions of CSTP5b: It was found that the uronic acid and neutral sugar contents in CSTP5b were 59.3 ± 0.17% and 85.59 ± 0.08%, respectively. A minor protein content of 0.8 ± 0.03% was observed, which suggested the effective removal of protein impurities during purification. As shown in Fig. 1(a), the ultraviolet–visible (UV-Vis) spectra of CSTP5b lacked absorption at 280 and 260 nm, which indicated that proteins and nucleic acids were absent.

The homogeneity and molecular weight distribution of CSTP5b were shown in Fig. 1b. A single symmetrical peak was detected, which implied the homogeneousness of CSTP5b. A linear equation with dextran standards of varying molecular weights was employed to determine the Mw and Mn of CSTP5b as 65.8 and 64.0 kDa, respectively. The polydispersity index (PDI, Mw/Mn) of 1.03 suggested a narrow molecular mass distribution for the homogeneous polysaccharide.

The monosaccharide composition of the hydrolyzed CSTP5b was identified (Figs. 1c-d). CSTP5b consisted of galacturonic acid (GalA) (57.88%), galactose (Gal) (20.71%), rhamnose (Rha) (13.11%) and arabinose (Ara) (8.3%) in comparison with monosaccharide standards (Figs. 1c-d). The presence of GalA proved that CSTP5b was an acidic heteropolysaccharide. Pectic polysaccharides are made up of various domains, primarily rhamnogalacturonan-I (RG-I) and homogalacturonan (HG).

The molar ratio of monosaccharide composition reflects the relative proportions of various pectin domains. The CSTP5b component is mainly constituted by RG-I (55.23%) and HG (44.77%) domains, as determined by monosaccharide composition analysis. Of note, the GalA proportion was much higher than that in prior research (Jing *et al.*, 2016; Ma *et al.*, 2024), which could be chiefly attributed to different extraction methods or raw materials. Traditional hot water extraction can only dissolve Ara, Gal and other water-soluble sugars from side chains of pectic polysaccharides. Nevertheless, ammonium oxalate is effective in dissociating the cross-linked network formed by GalA and Ca^{2+}, which is the reason for the relatively high content of GalA in CSTP5b.

Fourier transform infrared spectroscopy analysis: As shown in Fig. S2, CSTP5b showed a broad peak at 3,365 cm^{-1}, which indicated hydroxyl stretching vibration. C-H stretching vibrations were responsible for 2,933 cm^{-1} bands (Liu *et al.*, 2021). The bands of 1,739 and 1,610 cm^{-1} represented the stretching vibrations of methylated (-COOCH3) and free (-COO-) carboxyl groups in uronic acid, respectively (Gómez-Ordóñez & Rupérez, 2011). The DM of CSTP5b was calculated to 22.34% (DM＜50%) (Chen *et al.*, 2019). It can primarily be deduced that CSTP5b obtained through chelator extraction was low methoxyl pectin. Pyran configurations in CSTP5b were suggested by the absorption bands at 900~1,200 cm^{-1} (Hong *et al.*, 2022).

Morphological properties: Scanning electron microscopy (SEM) analysis was utilized for capturing the microstructure morphologies of CSTP5b. The images are depicted in Fig. 2(a-c). CSTP5b showed an irregular flake-like structure, and its surface was smooth with circular protrusions under 200× and 500× magnifications. It was noted that the surface became asperities with a number of small uneven particles under 5,000× magnification.

The crystallization characteristics of pectin significantly affect its mechanical strength, gel properties, as well as biodegradability. As illustrated in Fig. 2d, CSTP5b exhibits sharp and narrow diffraction peaks at 32.475° and 46.174° within the diffraction angle 2θ range of 5°-90°, which indicates that CSTP5b mainly exists in a weakly crystalline form. This may be ascribed to the ordered structure formed by the GalA linear backbone in the HG structural unit of pectic polysaccharide (Ponmurugan *et al.*, 2017).

As indicated in Figs. 2(e-f), the AFM planar and cubic spectra revealed a morphology of irregular flakes and blocks with a height of -4.8~6.9 nm. The CSTP5b diameter measured by AFM was larger than that of single chains of polysaccharides, which indicated the entanglement and aggregation of pectic polysaccharide chains. The aggregation of CSTP5b could result from hydrogen bonding within and between molecules on its surface, as well as interactions with water molecules (Camesano & Wilkinson, 2001; Wang & Nie, 2019).

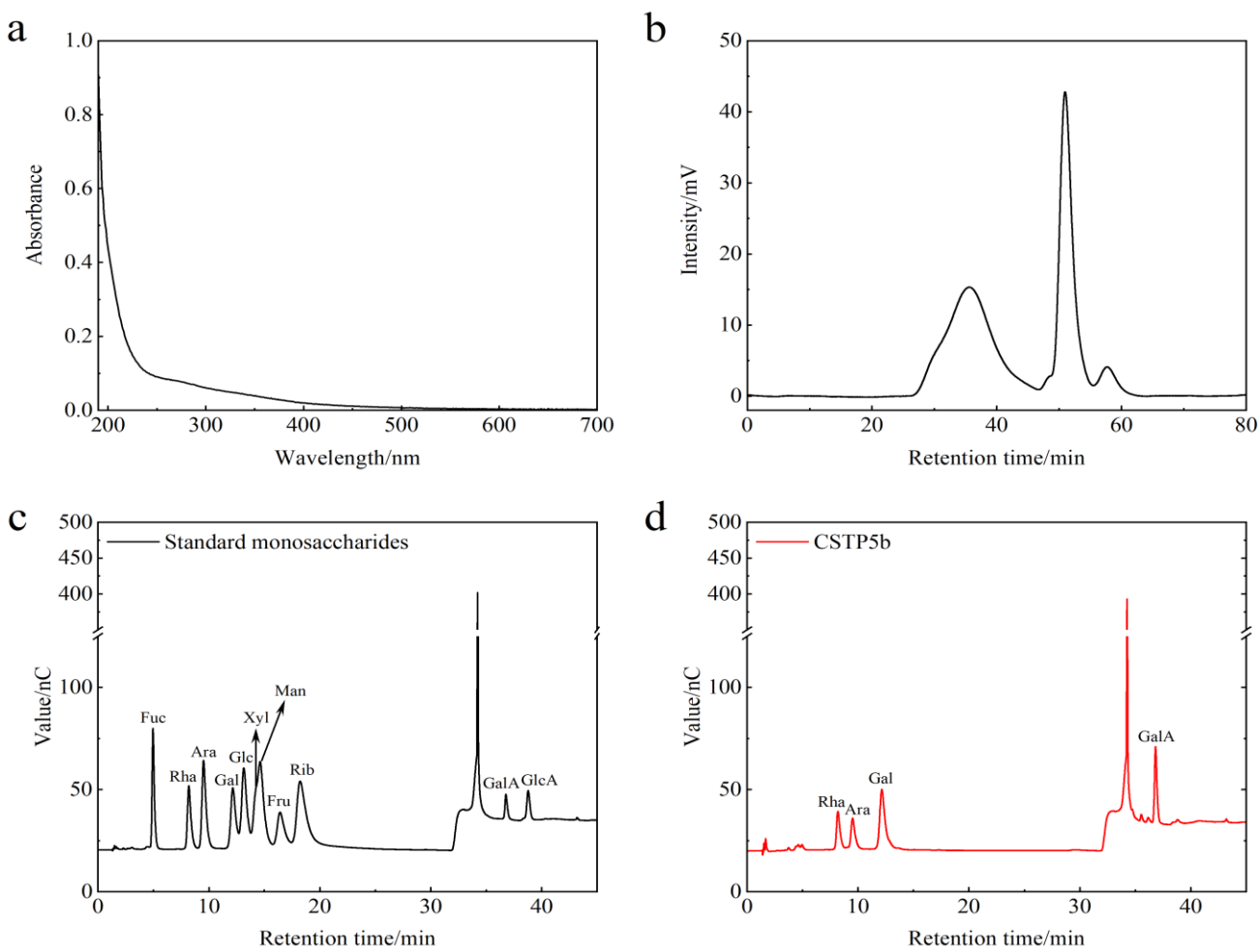

Fig. 1. (a) UV-Vis absorption spectra of CSTP5b; (b) HPGPC of CSTP5b; (c-d) Ion chromatogram of standard monosaccharides (c) and CSTP5b (d).

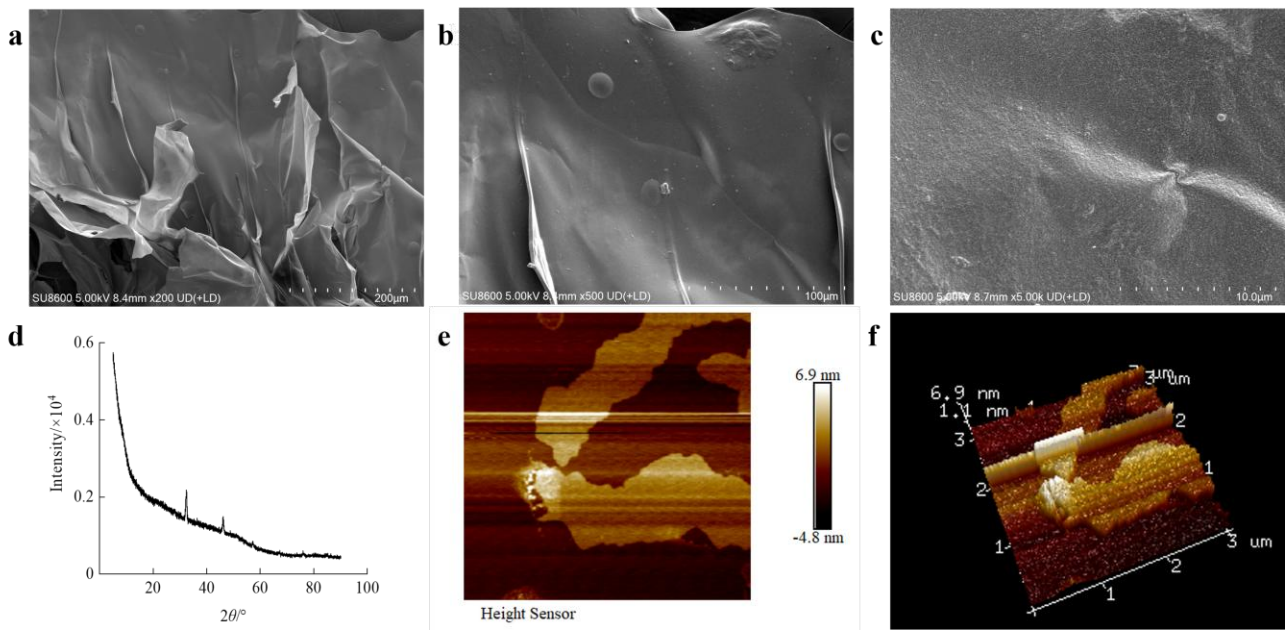

Fig. 2. Physicochemical analysis of CSTP5b. Surface morphology of CSTP5b observed under SEM at magnifications of 200× (a), 500× (b) and 5,000× (c). (d) XRD pattern of CSTP5b. (e-f) AFM planar (e) and cubic images (f) of CSTP5b (scan size: 5 μm)

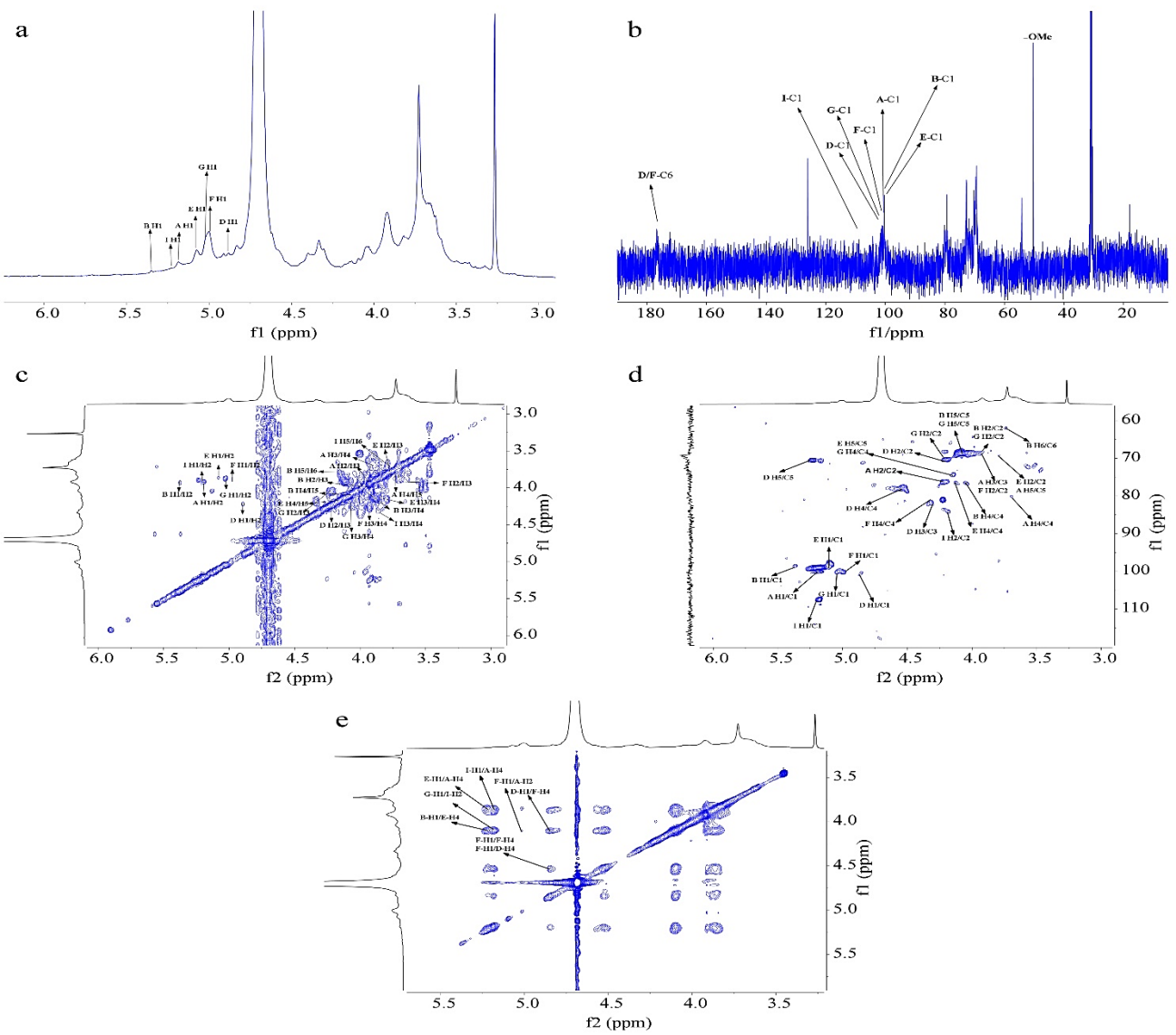

Fig. 3. NMR spectra of the pectic polysaccharide fraction CSTP5b. (a) ^{1}H NMR. (b) ^{13}C NMR. (c) COSY. (d) HSQC. (e) NOESY.

Table 1. Results of methylated glycyryl acetate (PMAA) of CSTP5b.

Peaks	Retention time (min)	Methylated sugar	Molar (%)	Glycosidic linkages
1	10.288	2,3,5–Me_3–Arap	3.3	Arap–(1→
2	14.835	3,5–Me_2–Araf	4.4	→2)–Araf–(1→
3	17.482	2,3,4,6–Me_4–Galp	7.0	Galp–(1→
4	18.650	3–Me_1–Rhap	4.0	→2,4)–Rhap–(1→
5	20.826	2,3,6–Me_3–Galp	57.7	→4)–Galp–(1→/→4)–GalpA–(1→
6	23.911	2,6–Me_2–Galp	17.2	→3,4)–Galp–(1→/→3,4)–GalpA–(1→
7	26.525	2,3–Me_2–Galp	6.4	→4,6)–Galp–(1→

Table 2. Assignments of hydrocarbon for CSTP5b.

	Glycosyl residues	H1/C1	H2/C2	H3/C3	H4/C4	H5a/C5	H6a,H5b/C6	H6b/C6
A	→2,4)–α–D–Rhap–(1→	5.19	4.24	3.9	3.73	3.82	1.25	
		100.37	77.69	69	77.9	71.9	18.1	
B	α–D–Galp–(1→	5.38	3.91	3.97	4.07	4.1	3.75	
		99.91	68.22	80.5	78.1	70.09	63.56	
D	→3,4)–α–D–GalpA–(1→	4.87	4.22	4.24	4.55	5.25		
		101.54	71.68	82.38	79.25	71.86	176.7	
E	→4,6)–α–D–Galp–(1→	5.1	3.75	3.84	4.14	4.16	4	4.01
		99.48	69.77	70.49	77.93	75.61	65.74	
F	→4)–α–D–GalpA–(1→	4.97	3.67	3.93	4.32	4.68		
		100.38	69.4	70.05	79.15	72.65	176.7	
G	α–Arap–(1→	5.02	4.22	4.05	4.2	3.58	3.65	
		101.3	69.53	71.46	73.11	63.73		
I	→2)–α–L–Araf–(1→	5.2	4.2	3.82	4.34	3.78	3.69	
		108.87	85.49	78.53	83.35	62.61		

Glycosidic linkage analysis: The glycosidic linkage patterns and mass fragment information are displayed in Table 1. Seven methylated glycyryl acetates (PMAAs) were found in CSTP5b based on the methylation analysis. CSTP5b primarily comprised →4)–Galp–(1→/→4)–GalpA–(1→ (57.7%), →3,4)–Galp–(1→/→3,4)–GalpA–(1→ (17.2%), Galp–(1→ (7.0%), →4,6)–Galp–(1→ (6.4%), →2)–Araf–(1→ (4.4%), →2,4)–Rhap–(1→ (4.0%) and Arap–(1→ (3.3%). The main structural component of CSTP5b was →4)–GalpA–(1→, as identified by monosaccharide composition. The branching degree was calculated as 37.9% as per the previous method (Tang *et al.*, 2021).

NMR analysis: NMR spectroscopy provides an efficient approach for acquiring detailed structural insights into complex polysaccharides. The NMR spectra of CSTP5b are presented in Fig. 3. The ^{1}H NMR spectrum (Fig. 3a) displayed signals mainly in the range of 3.0 to 5.5 ppm. In the ^{13}C NMR spectrum (Fig. 3b), a majority of signals appeared between 60 and 120 ppm. The NMR spectrum analysis of the CSTP5b head region showed chemical shifts at δ5.19/100.37, 5.38/99.91, 4.87/101.54, 5.1/99.48, 4.97/100.38, 5.02/101.3 and 5.2/108.87 ppm, designated as letters. As demonstrated in Fig. 3b, the uronic acid signal of 176.7 ppm was noticed. The attributions for each residue are detailed in Table 2. The monosaccharide composition results indicated that CSTP5b is a typical pectic polysaccharide.

A shift of H-1 to H-5 at δ4.97, 3.67, 3.93, 4.32 and 4.68 ppm is revealed in Fig. 2c. As shown in Fig. 3d, C-1 to C-5 signals were found at δ100.38, 69.4, 70.05, 79.15, and 72.65 ppm. As illustrated in Figure 3e, the cross peak at δ4.97/4.32 ppm corresponded to H1/H4. It suggests that residue F is →4)–α–D–GalpA–(1 →. Moreover, the H-3/C-3 signal (δ4.24/82.38) for residue D was noticeably downfield compared to that (δ3.93/70.05) for residue F, which suggested an O–3 substitution. Residue D is characterized as →3,4)-α-D-GalpA-(1→.

A similar approach was adopted to obtain the hydrogen and carbon signals of other primary residues. Residues were analyzed using the above analysis, in conjunction with prior studies (Liu *et al.*, 2024). Residue A is →2,4)–α–D–Rhap–(1→; residue B is α–D–Galp–(1→; residue E is →4,6)–α–D–Galp–(1→; residue G is α–Arap–(1→); residue I is →2)–α–L–Araf–(1→.

In the NOESY spectrum (Fig. 3e), the following cross-peaks were noted: F H-1/F H-4, F H-1/D H-4, F H-1/A H-2, G H-1/I H-2, B H-1 to E H-4, E H-1 to A H-4 and I H-1 to A H-4.

Based on the analysis, CSTP5b was identified as an RG-I-HG pectin with a primary chain of →[4)–α–D–GalpA–(1]$_6$→4)–α–D–GalpA(OMe)–(1→4)–α–D–GalpA–(1→2)–α–D–Rhap–(1→4)–α–D–GalpA–(1→2)–α–D–Rhap–(1→. The side chain includes branches of α–L–Arap–(1→2)–α–L–Araf–(1→ and α–D–Galp–(1→4,6)–α–D–Galp–(1→, linked via →2,4)–α–L–Rhap–(1→ at the O–4 position, with a minor presence of α–D–Galp–(1→. The predicted structure of CSTP5b is illustrated in Fig. 4.

Thermal stability: TG analysis (TGA) and DSC were used to evaluate the thermal behavior of pectic polysaccharides. As indicated in Fig. S3(a), the TG

analysis of tobacco pectic polysaccharides revealed three stages of decomposition. The initial phase saw a mass reduction of 16% because of moisture loss (Einhorn-Stoll & Kunzek, 2009). During the second stage (166~516℃), CSTP5b experienced significant weight loss (up to 60%) owing to thermal decomposition. The process entailed the cleavage of glycosidic bonds, the decarboxylation of acid groups and the breakdown of C-C bonds in the pyran ring, which resulted in the formation of solid char (Hu *et al.*, 2020). The third stage (516~800℃) showed a slow weight reduction, which implied the further breakdown of carbonized substances with aliphatic and ketone groups (Zhou *et al.*, 2011). The DSC curve in Fig. S3(b) indicated that CSTP5b exhibited endothermic behavior from 40-340℃ due to the loss of bound water. Concurrently, this process was accompanied by pectic polysaccharide dehydroxylation and conformational changes, like the transition of polygalacturonic acid from a stable $^4C_1$ chair conformation to a thermodynamically less stable inverted $^1C_4$ chair conformation (Wani & Uppaluri, 2023). Furthermore, an exothermic phenomenon was observed between 340℃ and 800℃. This was potentially associated with the thermal degradation of pectin polysaccharides. These results verified the exceptional thermal stability of CSTP5b.

Antioxidant activity: Vc was used as a reference to assess the scavenging capabilities of CSTP5b against DPPH, hydroxyl radical (·OH) and ABTS (Figs. 5a-c). The activity showed a progressive increase with the increase of concentration levels, which indicated a dose-dependent effect. In the DPPH radical assay (Fig. 5a), CSTP5b demonstrated marked antioxidant activity with a radical scavenging rate of 65.96 ± 1.35% (8 mg/mL). CSTP5b exhibited a scavenging effect of 48.27 ± 1.92% on ·OH radicals at 8 mg/mL (Fig. 5b). CSTP5b demonstrated ABTS radical scavenging activity across all the tested concentrations, with scavenging rates of 21.47 ± 2.27%, 26.63 ± 1.39%, 32.26 ± 1.51%, 55.18 ± 1.92%,62.85 ± 1.39% and 68.32 ± 1.51% at 0.5, 1, 2, 4, 6 and 8 mg/mL, respectively (Fig. 5c). The half maximal inhibitory concentration (IC_{50}) values were 4.40, 8.27 and 3.36 mg/mL, respectively. Hong et al. found that ASP-3A pectic polysaccharides derived from soybean hulls exhibit strong antioxidant activity by virtue of their low esterification degree and high GalA content (Song *et al.*, 2022). In this study, CSTP5b, a low methyl-esterified HG-type pectic polysaccharide, is primarily composed of GalA (65.4%), Rha (21.8%), and Ara (12.8%) in light of monosaccharide composition. Taken together with the structural analysis results, the high antioxidant activity of CSTP5b may originate from two possible reasons. One possible reason is that a low esterification degree (DM = 22.34%) enhances the hydrophilicity of pectin. The other possible reason is that high GalA content (> 60%) contributes hydrogen atoms or electrons through carboxyl and hydroxyl groups, which thereby neutralizes the effects of oxidative stress.

Hypoglycemic effects: Both α-glucosidase and α-amylase inhibition assays offer a simple and efficient approach for the evaluation of in vitro hypoglycemic activity. As demonstrated in Figs. 6(a-b), CSTP5b inhibited α-glucosidase and α-amylase in a concentration-dependent way (0.5~8 mg/mL). It exhibited a maximum inhibition rate of 43.82% on α-glucosidase and 35.86% on α-amylase. Both maximum inhibition rates were below those observed with acarbose in the positive control group. The IC_{50} values were 7.00 (α-glucosidase) and 9.09 mg/mL (α-amylase). CSTP5b exhibited superior inhibitory effects compared with certain known natural polysaccharides, like Lycium barbarum leaves polysaccharide (IC_{50} over 14.92 mg/mL) (Quan *et al.*, 2023) and Fructus Mori polysaccharide (IC_{50} 19.31 mg/mL) (Zhang *et al.*, 2019). The glycan chains of CSPT5b may encompass hydroxyl and carboxyl groups capable of interacting with amino acid residues, which leads to the inhibition of enzyme activity (Amamou *et al.*, 2020). Nonetheless, further research is warranted to explore CSTP5b as a potential hypoglycemic agent or alternative.

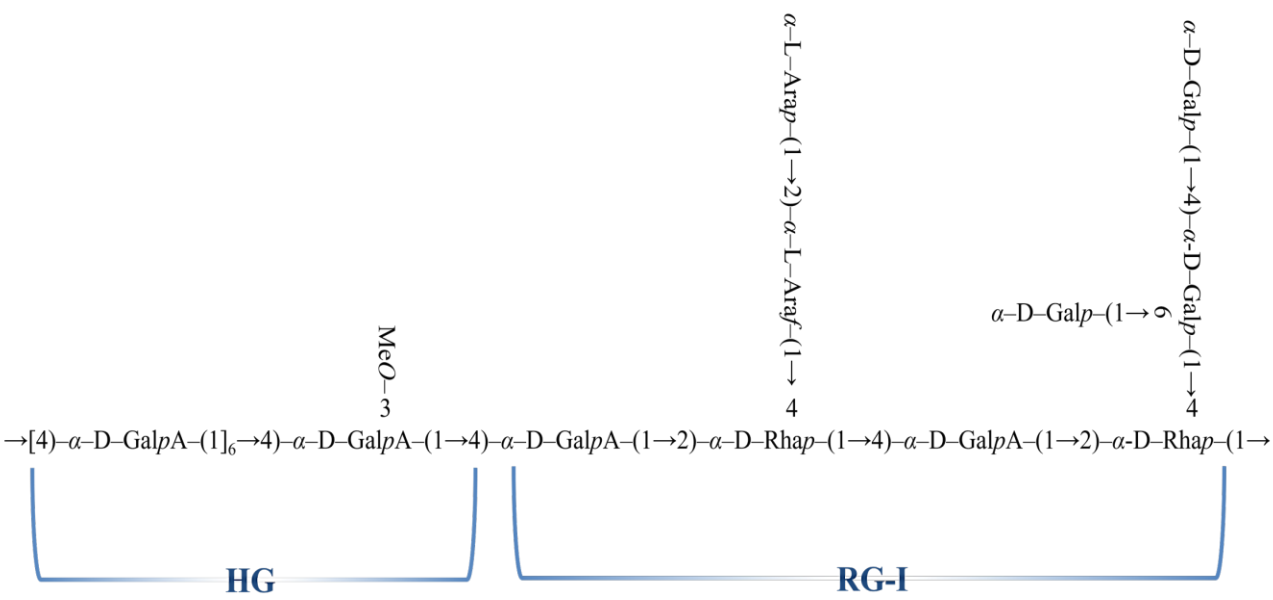

Fig. 4. Predicted structural repeating unit of CSTP5b.

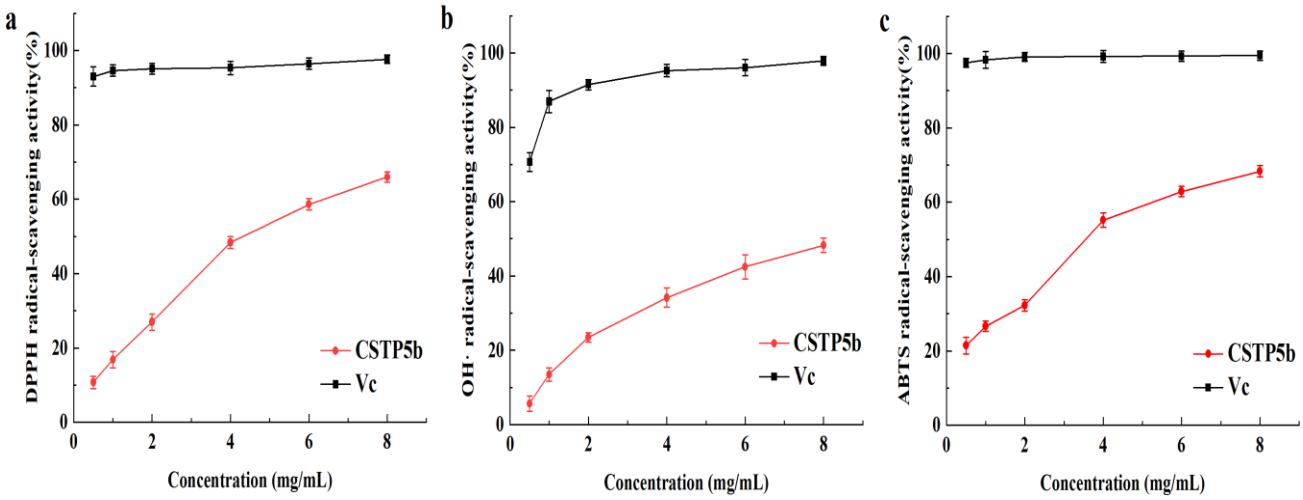

Fig. 5. (a) DPPH, (b) Hydroxyl and (c) ABTS free radical scavenging capacity of CSTP5b.

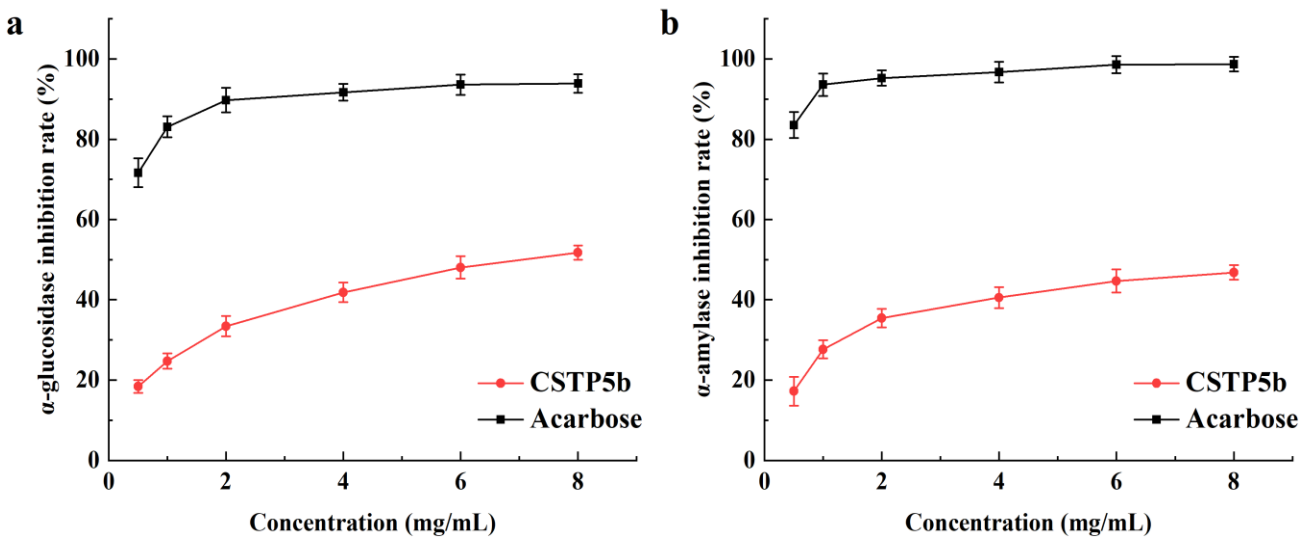

Fig. 6. (a) α-glucosidase and (b) α-amylase inhibition assays of CSTP5b.

Conclusion

The ammonium oxalate fractional extraction method was employed to extract pectic polysaccharide CSTP5b with a molecular weight of 65.8 kDa from tobacco waste. In this study, the physicochemical properties, structural characteristics and activities of CSTP5b were evaluated. This structure indicates that CSTP5b is a pectic polysaccharide consisting of RG-I (55.23%) and HG (44.77%) domains. Moreover, CSTP5b showed scavenging ability on free radicals and hypoglycemic activity. These findings provide a theoretical basis for the creation of beneficial functional ingredients from pectic polysaccharides in tobacco waste.

Competing interests: The authors have no relevant financial or non-financial interests to disclose.

Acknowledgment

Acknowledgment is given for the support from the Postdoctoral Project of Fujian Tobacco Industry Co., Ltd. (FJZYKJJH2023BH002).

References

Amamou, S., H. Lazreg, J. Hafsa, H. Majdoub, C. Rihouey, D. Le Cerf and L. Achour. 2020. Effect of extraction condition on the antioxidant, antiglycation and α-amylase inhibitory activities of *Opuntia macrorhiza* fruit peels polysaccharides. *LWT*, 127: 109411.

Braccini, I. and S. Pérez. 2001. Molecular basis of Ca^{2+}-induced gelation in alginates and pectins: The egg-box model revisited. *Biomacromolecules*, 2(4): 1089-1096.

Camesano, T.A. and K.J. Wilkinson. 2001. Single molecule study of xanthan conformation using atomic force microscopy. *Biomacromolecules*, 2(4): 1184-1191.

Cardoso, S.M., M.A. Coimbra and J.A. Lopes da Silva. 2003. Temperature dependence of the formation and melting of pectin–Ca^{2+} networks: A rheological study. *Food Hydrocol.*, 17(6): 801-807.

Chang, S., X. Lei, Q. Xie, M. Zhang, Y. Zhang, J. Xi, J. Duan, J. Ge and F. Nian. 2024. In vitro study on antioxidant and lipid-lowering activities of tobacco polysaccharides. *Bioresour. Bioproc.*, 11(1): 15.

Chen, X., Y. Qi, C. Zhu and Q. Wang. 2019. Effect of ultrasound on the properties and antioxidant activity of hawthorn pectin. *Int. J. Biol. Macromol.*, 131: 273-281.

Cui, J., C. Zhao, S. Zhao, G. Tian, F. Wang, C. Li, F. Wang and J. Zheng. 2020. Alkali + cellulase-extracted citrus pectins exhibit compact conformation and good fermentation properties. *Food Hydrocol.*, 108: 106079.

Docheva, M., S. Dagnon and S. Statkova-Abeghe. 2014. Flavonoid content and radical scavenging potential of extracts prepared from tobacco cultivars and waste. *Nat. Prod. Res.*, 28(17): 1328-1334.

Einhorn-Stoll, U. and H. Kunzek. 2009. Thermoanalytical characterisation of processing-dependent structural changes and state transitions of citrus pectin. *Food Hydrocol.*, 23(1): 40-52.

Gómez-Ordóñez, E. and P. Rupérez. 2011. FTIR-ATR spectroscopy as a tool for polysaccharide identification in edible brown and red seaweeds. *Food Hydrocol.*, 25(6): 1514-1520.

Hao, J., X. Wang, Y. Chai, X. Huang, H. Wu, S. Zhang, X. Duan and L. Qin. 2024. Evaluation of lipid and metabolite profiles in tobacco leaves from different plant parts by comprehensive lipidomics and metabolomics analysis. *Ind. Crops Prod.*, 212: 118318.

Ho, G.T.T., Y.F. Zou, H. Wangensteen and H. Barsett. 2016. RG-I regions from elderflower pectins substituted on gala are strong immunomodulators. *Int. J. Biol. Macromol.*, 92: 731-738.

Hong, T., J. Zhao, J. Yin, S. Nie and M. Xie. 2022. Structural characterization of a low molecular weight HG-type pectin from gougunao green tea. *Front. Nutr.*, 9: 878249.

Hu, W., X. Ye, T. Chantapakul, S. Chen and J. Zheng. 2020. Manosonication extraction of RG-I pectic polysaccharides from citrus waste: Optimization and kinetics analysis. *Carbohydr. Polym.*, 235: 115982.

Huang, L., Q. Sun, Q. Li and X. Li. 2024. Screening and characterization of an anti-inflammatory pectic polysaccharide from *Cucurbita moschata* Duch. *Int. J. Biol. Macromol.*, 264: 130510.

Huang, L., J. Zhao, Y. Wei, G. Yu, F. Li and Q. Li. 2021. Structural characterization and mechanisms of macrophage immunomodulatory activity of a pectic polysaccharide from *Cucurbita moschata* Duch. *Carbohydr. Polym.*, 269: 118288.

Jamsazzadeh Kermani, Z., A. Shpigelman, C. Kyomugasho, S. Van Buggenhout, M. Ramezani, A.M. Van Loey and M.E. Hendrickx. 2014. The impact of extraction with a chelating agent under acidic conditions on the cell wall polymers of mango peel. *Food Chem.*, 161: 199-207.

Jing, Y., Y. Gao, W. Wang, Y. Cheng, P. Lu, C. Ma and Y. Zhang. 2016. Optimization of the extraction of polysaccharides from tobacco waste and their biological activities. *Int. J. Biol. Macromol.*, 91: 188-197.

Kang, Y.R. and Y.H. Chang. 2024. Structural and flow rheological properties of pumpkin pectic polysaccharide extracted by citric acid. *Int. J. Biol. Macromol.*, 265: 130748.

Kang, Y.R. and Y.H. Chang. 2024. Structural characterization and prebiotic activity of rhamnogalacturonan-I rich pumpkin pectic polysaccharide extracted by alkaline solution. *Int. J. Biol. Macromol.*, 270: 132311.

Liu, F., X. Zhang, M. Wang, L. Guo, Y. Yang and M. Zhao. 2020. Biosorption of sterols from tobacco waste extract using living and dead of newly isolated fungus *Aspergillus fumigatus* strain LSD-1. *Biosci., Biotechnol., Biochem.*, 84(7): 1521-1528.

Liu, Y., Y. Meng, H. Ji, J. Guo, M. Shi, F. Lai and X. Ji. 2024. Structural characteristics and antioxidant activity of a low-molecular-weight jujube polysaccharide by ultrasound assisted metal-free fenton reaction. *Food Chem.,* 24: 101908.

Liu, Y., Y. Ye, X. Hu and J. Wang. 2021. Structural characterization and anti-inflammatory activity of a polysaccharide from the lignified okra. *Carbohydr. Polym.*, 265: 118081.

Ma, M., X. Long, Y. Wang, K. Chen, M. Zhao, L. Zhu and Q. Chen. 2024. Synergized enzyme-ultrasound-assisted aqueous two-phase extraction and antioxidant activity validation of polysaccharides from tobacco waste. *Microchem. J.*, 202: 110799.

Ma, R., T. Cao, H. An, S. Yu, H. Ji and A. Liu. 2023. Extraction, purification, structure, and antioxidant activity of polysaccharide from *Rhodiola rosea*. *J. Mol. Struct.*, 1283: 135310.

Ning, X., Y. Liu, M. Jia, Q. Wang, Z. Sun, L. Ji, K.H. Mayo, Y. Zhou and L. Sun. 2021. Pectic polysaccharides from Radix *Sophorae Tonkinensis* exhibit significant antioxidant effects. *Carbohydr. Polym.*, 262: 117925.

Peng, Y., Z. Zhang, W. Chen, S. Zhao, Y. Pi and X. Yue. 2023. Structural characterization, α-glucosidase inhibitory activity and antioxidant activity of neutral polysaccharide from apricot (*Armeniaca Sibirica* L. Lam) kernels. *Int. J. Biol. Macromol.*, 238: 124109.

Ponmurugan, K., N.A. Al-Dhabi, J.P. Maran, K. Karthikeyan, I.G. Moothy, N. Sivarajasekar and J.J.B. Manoj. 2017. Ultrasound assisted pectic polysaccharide extraction and its characterization from waste heads of *Helianthus annus*. *Carbohydr. Polym.*, 173: 707-713.

Quan, N., Y.D. Wang, G.R. Li, Z.Q. Liu, J. Feng, C.L. Qiao and H.F. Zhang. 2023. Ultrasound–microwave combined extraction of novel polysaccharide fractions from *Lycium barbarum* leaves and their *In vitro* hypoglycemic and antioxidant activities. *Molecules*, 28(9): 3880.

Song, H., L. Han, Z. Zhang, Y. Li, L. Yang, D. Zhu, S. Wang, Y. He and H. Liu. 2022. Structural properties and bioactivities of pectic polysaccharides isolated from soybean hulls. *LWT*, 170: 114079.

Sun, H., R.Z. Chen, F.L. Meng, H.L. Bai, L. Tian, J. Lu, C.L. Bai, D.X. Li, W.J. Wu, Y.T. Wang and M.Z. Gong. 2024. Extraction, characterization, antioxidant and hypoglycemic of pectic polysaccharides from cantaloupe (*Cucumis melo* L.) peels. *Starch-Stärke*, 76: 2300157.

Tang, W., D. Liu, Y. Li, M.Y. Zou, Y.C. Shao, J.Y. Yin and S.P. Nie. 2021. Structural characteristics of a highly branched and acetylated pectin from *Portulaca oleracea* L. *Food Hydrocol.*, 116: 106659.

Teng, C., P. Qin, Z. Shi, W. Zhang, X. Yang, Y. Yao and G. Ren. 2021. Structural characterization and antioxidant activity of alkali-extracted polysaccharides from quinoa. *Food Hydrocol.*, 113: 106392.

Tian, W.W., F. Xu, S.J. Xing, R. Wu and Z.Y. Yuan. 2023. Comprehensive study on the thermal decomposition process of waste tobacco leaves and stems to investigate their bioenergy potential: Kinetic, thermodynamic, and biochar analysis. *Thermoch. Acta*, 723: 179473.

Wang, H., M. Zhao, B. Yang, Y. Jiang and G. Rao. 2008. Identification of polyphenols in tobacco leaf and their antioxidant and antimicrobial activities. *Food Chem.*, 107(4): 1399-1406.

Wang, J. and S. Nie. 2019. Application of atomic force microscopy in microscopic analysis of polysaccharide. *Trends Food Sci. Technol.*, 87: 35-46.

Wang, W., J. Yao and X. Cao. 2022. Alkaloids from tobacco leaves: Isolation, alkaloid contents, and potential application as a natural pesticide against *Bactrocera dorsalis*. *Bioresources*, 17(1): 1764-1780.

Wang, Y. and W. Gu. 2018. Study on supercritical fluid extraction of solanesol from industrial tobacco waste. *J. Supercrit. Fluids*, 138: 228-237.

Wani, K.M. and R.V.S. Uppaluri. 2023. Characterization of pectin extracted from pomelo peel using pulsed ultrasound assisted extraction and acidic hot water extraction process. *Appl. Food Res.*, 3(2): 100345.

Yang, M., Z. Liu, J. Zhang, X. Zhu, W. Xie, H. Lan, Y. Huang, X. Ye and J. Yang. 2022. Simultaneous quantification of cellulose and pectin in tobacco using a robust solid-state NMR method. *Carbohydr. Res.*, 521: 108676.

Zhang, J.Q., C. Li, Q. Huang, L.J. You, C. Chen, X. Fu and R.H. Liu. 2019. Comparative study on the physicochemical properties and bioactivities of polysaccharide fractions extracted from *Fructus Mori* at different temperatures. *Food Funct.*, 10(1): 410-421.

Zhou, S., Y. Xu, C. Wang and Z. Tian. 2011. Pyrolysis behavior of pectin under the conditions that simulate cigarette smoking. *J. Anal. Appl. Pyrolysis*, 91(1): 232-240.